Atmos. Chem. Phys. Discuss., 14, 4787–4826, 2014
www.atmos-chem-phys-discuss.net/14/4787/2014/
doi:10.5194/acpd-14-4787-2014

Atmospheric Chemistry and Physics Discussions

Fog scavenging of organic and inorganic aerosol in the Po Valley

S. Gilardoni[1], P. Massoli[4], L. Giulianelli[1], M. Rinaldi[1], M. Paglione[1], F. Pollini[1], C. Lanconelli[1], V. Poluzzi[2], S. Carbone[3], R. Hillamo[3], L. M. Russell[5], M. C. Facchini[1], and S. Fuzzi[1]

[1]Italian National Research Council – Institute of Atmospheric Sciences and Climate, Bologna, Italy
[2]ARPA Emilia Romagna, Bologna, Italy
[3]Finnish Meteorological Institute, Helsinki, Finland
[4]Aerodyne Research, Billerica, MA, USA
[5]Scripps Institute of Oceanography, La Jolla, CA, USA

Received: 19 December 2013 – Accepted: 24 January 2014 – Published: 21 February 2014

Correspondence to: S. Gilardoni (s.gilardoni@isac.cnr.it)

Published by Copernicus Publications on behalf of the European Geosciences Union.

Abstract

The interaction of aerosol with atmospheric water affects the processing and wet removal of atmospheric particles. Understanding such interaction is mandatory to improve model description of aerosol lifetime and ageing. We analyzed the aerosol-water interaction at high relative humidity during fog events in the Po Valley, in the framework of the ARPA-ER Supersite project. For the first time in this area, the changes in particle chemical composition caused by fog are discussed along with changes in particle microphysics.

During the experiment, 14 fog events were observed. The average mass scavenging efficiency was 70 % for nitrate, 68 % for ammonium, 61 % for sulfate, 50 % for organics, and 39 % for black carbon. After fog formation, the interstitial aerosol was dominated by particles smaller than 200 nm D_{va} (vacuum aerodynamic diameter) and enriched in carbonaceous aerosol, mainly black carbon and water insoluble organic aerosol (WIOA).

For each fog event, the size segregated scavenging efficiency of nitrate and organic aerosol (OA) was calculated by comparing chemical species size distribution before and after fog formation. For both nitrate and OA, the size segregated scavenging efficiency followed a sigmoidal curve, with values close to zero below 100 nm D_{va} and close to 1 above 700 nm D_{va}. OA was able to affect scavenging efficiency of nitrate in particles smaller than 300 nm D_{va}. A linear correlation between nitrate scavenging and particle hygroscopicity (κ) was observed, indicating that 44–51 % of the variability of nitrate scavenging in smaller particles (below 300 nm D_{va}) was explained by changes in particle chemical composition.

The size segregated scavenging curves of OA followed those of nitrate, suggesting that organic scavenging was controlled by mixing with water-soluble species. In particular, functional group composition and OA elemental analysis indicated that more oxidized OA was scavenged more efficiently than less oxidized OA. Nevertheless, the small variability of organic functional group composition during the experiment did not allow us to discriminate the effect of different organic functionalities on OA scavenging.

ACPD
14, 4787–4826, 2014

1 Introduction

Fog scavenging is the process by which atmospheric particles transfer into the liquid phase of fog droplets. Fog scavenging affects particle microphysical and chemical properties, which are relevant to predict the effect of aerosol on climate and air quality. Indeed, fog scavenging reduces aerosol loading by promoting wet removal (Collett et al., 2001), and modifies aerosol hygroscopicity and particle size distribution by selectively removing water soluble species (Collett et al., 2008). In addition, particle water uptake associated with fog promotes aerosol processing and secondary aerosol formation through heterogeneous phase chemistry (Kaul et al., 2011; Ervens et al., 2011; Li et al., 2013).

Fog scavenging can take place through both impaction scavenging and nucleation scavenging. Impaction scavenging occurs when interstitial particles are incorporated into fog droplets as a consequence of Brownian diffusion, inertial impaction, and phoretic effect. In a supersaturated atmosphere, aerosol particle can be activated to form fog droplets and be scavenged by nucleation. Generally, nucleation scavenging dominates in-cloud and in-fog aerosol scavenging (Seinfeld and Pandis, 1998; Elbert et al., 2000).

Several fog experiments proved that nucleation scavenging is the dominant aerosol scavenging mechanism in the Po Valley. Fuzzi et al. (1988) observed that sulfate scavenging efficiency was lower compared to in-cloud measurements and attributed this difference to the lower supersaturation of fog compared to clouds. In the same area Hallberg et al. (1992) observed that fog scavenging efficiency of different chemical compounds was related to their water solubility, with higher scavenging for water soluble species, like sulfate, and lower for carbonaceous hydrophobic compounds, like elemental carbon. During the same experiment, the comparison of particle number size distribution in and out of fog showed that fog scavenging did not affect smaller particle concentration (mobility diameter D_m below 300 nm), but removed efficiently particles larger than 700 nm D_m, leading to the conclusion that aerosol scavenging was mainly

ACPD
14, 4787–4826, 2014

driven by nucleation (Noone et al., 1992). Elbert et al. (2000) investigated the relationship between atmospheric liquid water content and chemical composition of fog-water samples, and concluded that nucleation scavenging was the dominant particle removal mechanism.

The critical supersaturation required to nucleate fog droplets is usually around 0.01 and 0.03 % (Noone et al., 1992; Ming and Russell, 2004). However, in highly polluted environments like the Po Valley, soluble species in the gas phase and organic solutes in the liquid droplets might decrease the critical supersaturation required for particle activation, making possible cloud and fog formation even at ambient relative humidity below 100 % (Shulman et al., 1996; Laaksonen et al., 1998; Facchini et al., 1999b).

Although an increasing number of experiments investigated nucleation at supersaturation typical of clouds, little is known about the relative importance of chemistry and microphysics on Cloud Condensation Nuclei (CCN) activity at supersaturation close to zero, which is typical of fog. Some studies show that particle size explained more than 84 % of the CCN variability at a supersaturation of 0.4 %. (Dusek et al., 2006). Other studies instead suggest that particle chemical composition can explain 40 % of the critical diameter variability at a supersaturation of 0.44 %; at lower supersaturation the influence of particle composition is expected to be even higher (Quinn et al., 2008). More recently, observations performed during a wide number of aircraft campaigns and ground based experiments led to the conclusion that both size and compositional information are required to predict particle CCN activity (Hudson, 2007; Levin et al., 2013).

At the same time, the effect of fog scavenging on particle chemical composition, and especially on OA, is still poorly understood (Herckes et al., 2007). Facchini et al. (1999a) studied the distribution of different classes of carbonaceous species between interstitial aerosol and fog water, reporting a preferential partitioning of water soluble organic carbon in fog droplets. Even when impaction scavenging is the dominant mechanism, a preferential removal of hydrophilic organic species was observed (Maria and Russell, 2005). Collett et al. (2008) investigated organic aerosol scavenged during four

ACPD
14, 4787–4826, 2014

fog events in central California and observed a slight positive correlation with liquid water content (LWC). However, no information on particle microphysics and mixing state with other chemical constituents were available in these studies.

This paper analyzes the fog scavenging efficiency of major chemical components in fine particles through field observations in the Po Valley during fall of 2011, in the framework of the ARPA-Emilia Romagna Supersite project. For the first time in this area, the effects of fog on particle chemistry were investigated at high time resolution and taking into account particle microphysics. The objective of this study is to analyze the effect of scavenging on the chemical and the microphysical properties of aerosol after fog dissipation, and to investigate the role of chemical composition and mixing state of fine particles on nitrate scavenging and OA scavenging. In particular, scavenging of nitrate and OA is quantitatively discussed as a function of size distribution of the different chemical components and organic functional group composition.

2 Methods

2.1 Sampling site

The measurements described in this work were performed at the Meteorological station Giorgio Fea in San Pietro Capofiume, a rural background site located at about 30 km north-east of Bologna, in the eastern Po Valley (Northern Italy). Aerosol characterization was performed from 14 November to 1 December 2011. In the Po Valley, fall is usually characterized by stable meteorological conditions, with high relative humidity and low temperature, that lead to frequent fog events that often last for several hours (Fuzzi et al., 1992).

The meteorological conditions observed during the measurement period are reported in Fig. 1. High pressure and stable weather conditions characterized the entire campaign. Winds were generally below 2 $m\,s^{-1}$ and temperature averaged 3 °C, with values around 10 °C during daytime and 0 °C at night-time. Relative humidity (RH)

ACPD
14, 4787–4826, 2014

was often close to 100 % throughout both daytime and night-time, especially before 23 November.

Liquid water content (LWC) was measured continuously with a Particulate Volume Monitor PVM-100 (Gerber, 1991) at one minute time resolution. LWC higher than 0.08 g L^{-1} is an indicator of fog presence. LWC time trend is reported in Fig. 2a and indicates that fog formed almost every evening, around 17:00 local time (LT), and persisted during great part of the night till the following morning, to disappear around 09:00 LT. During the entire campaign a total of 14 distinct fog events were identified.

2.2 Aerosol sampling

Size segregated aerosol particles were sampled by a Berner impactor (flow rate 80 L min^{-1}) on aluminum and Tedlar foils. The Berner impactor collects particles on five stages, corresponding to the following particle aerodynamic diameter cut-offs: 0.14, 0.42, 1.2, 3.5, and 10 µm. Sampling was performed continuously during the entire period. Each day we collected two samples: a daytime sample from 09:00 to 17:00 LT, and a night-time one from 17:00 to 09:00 LT. Particles collected on aluminum foils were analyzed for carbonaceous aerosol content by thermal technique, while samples collected on Tedlar were analyzed by ion chromatography for quantification of water soluble inorganic species.

Submicron particles were collected on Teflon filters (37 mm diameter) downstream of a silica gel drier and a PM_1 cut cyclone (flow rate 16.7 L min^{-1}). One 24 h sample was collected daily from 09:00 to 09:00 LT. Three additional samples were collected each day from 09:00 to 13:00, from 13:00 to 17:00 and from 17:00 to 09:00 of the following morning.

Submicron particles were also sampled on pre-washed and pre-baked quartz-fiber filters (PALL, 9 cm size) using a dichotomous sampler (Universal Air Sampler, model 310, MSP Corporation) at a constant nominal flow of 300 L min^{-1} located at ground level. A total of thirty samples were collected between 15 and 30 November. Typically, two filters were sampled every day, with a daytime PM_1 sample collected from 09:00 to

ACPD
14, 4787–4826, 2014

17:00 LT, and an evening/night-time sample collected from 18:00 to 09:00 LT. Samples were stored in petri dishes at 4 °C prior to analysis.

2.3 Off-line aerosol chemical characterization

Size segregated concentrations of inorganic ions were measured by ion chromatography analysis of ultrapure water extracts of Tedlar substrates.

Water soluble organic carbon (WSOC) was detected by analyzing the Tedlar substrate water extracts by a Multi N/C 2100S (Analytik Jena, Germany) elemental analyzer. WSOC was quantified as the difference between total water soluble carbon and soluble inorganic carbon. Total Carbon (TC) was determined by the analysis of aluminum foil by the same technique. The detection limit was 0.2 µg of carbon and the accuracy of the TC measurement was better than 5 % for 1 µg of carbon.

The dichotomous quartz-fiber filters were analyzed to identify organic molecular tracers using proton nuclear magnetic resonance (HNMR) spectroscopy according to Decesari et al. (2006).

Organic aerosol functional groups were analyzed by infrared spectrometry (Gilardoni et al., 2009; Russell et al., 2011). Teflon filters were analyzed by Fourier Transform Infrared (FTIR) Spectrometry in transmission mode in the region 400–4000 cm^{-1}, using a Bruker Tensor 27 FTIR Spectrometer, equipped with a deuterated triglycine sulfate (DTGS) detector. Spectrum resolution was 4 cm^{-1}. Filters were scanned prior and after aerosol collection, in order to remove Teflon absorption signals from the aerosol absorption spectrum. Aerosol spectra were then processed with an automated algorithm to perform baseline, peak-fitting, and peak integration, according to the procedure described by Russell et al. (2009). The functional group identified during the experiment include alkyl (-CH_2-), carboxyl (-COOH), hydroxyl (-OH), amine (-NH-), organonitrate (C-NO_3) groups. Aromatic and unsaturated aliphatic (=CH-), carbonyl (C=O), and organosulfate (C-OSO_3) moieties were below detection limit all the time. Absorption intensity was converted into mass according to Lambert–Beer equation, and based on calibration with standard representative of atmospheric aerosol organic molecules.

ACPD
14, 4787–4826, 2014

Organic mass was defined as the sum of the different organic functional groups. Elemental composition of organic aerosol was instead determined based on the elemental composition of each group.

2.4 On-line aerosol chemical characterization

The size-resolved chemical composition of submicron aerosol particles was characterized on-line by a High Resolution Time of Flight Aerosol Mass Spectrometer (HR-TOF-AMS) (DeCarlo et al., 2006) and a Soot Particle Aerosol Mass Spectrometer (SP-AMS) (Onasch et al., 2012).

The HR-TOF-AMS provided size resolved chemical measurements of the non - refractory sulfate, nitrate, ammonium, chloride, and organic mass in submicron particles (NR-PM_1). The HR-TOF-AMS was operating by alternating between "V" (higher sensitivity, lower mass resolution) and "W" (lower sensitivity, higher mass resolution) ion path modes every 5 min. The concentrations reported here correspond to the data collected in V-mode. While operating in V-mode, the HR-TOF-AMS acquires information about size distribution of particles, or particle time of flight (pToF) (Jimenez et al., 2003). The AMS has an effective 50 % cut-off for particle sizes below 80 and above 600 nm in vacuum aerodynamic diameter, D_{va}, as determined by the transmission characteristics of the standard aerodynamic lens (Liu et al., 2007). All data were analyzed using standard AMS software SQUIRREL v1.51 and PIKA v1.10 (D. Sueper, University of Colorado-Boulder, Boulder, CO, USA) within Igor Pro 6.2.1 (WaveMetrics, Lake Oswego, OR). Positive matrix factorization (PMF) analyses on the HR-AMS data were performed using the PMF2.exe algorithm (v.4.2) in robust mode (Paatero and Tapper, 1994). The PMF inputs (mass spectral and error matrices) were prepared according to Zhang et al. (2011). The PMF solutions were then evaluated with an Igor Pro-based PMF Evaluation Tool (PET, v. 2.04), following the method described in Ulbrich et al. (2009) and Zhang et al. (2011). The HR-TOF-AMS collection efficiency (CE) was calculated according to Middlebrook et al. (2011) and averaged 0.48 ± 0.05. Concentration

ACPD
14, 4787–4826, 2014

of AMS sulfate, nitrate, and ammonium corrected for CE and averaged over Berner impactor sampling periods were in agreement with off-line measurements.

The SP-AMS was operated with both the laser and the tungsten vaporizers, alternating the laser on and off every 10 min. The rBC data reported here are obtained in "laser on" mode, which provides measurements of the refractory component of the submicron aerosols, nominally rBC, and of the non-refractory coating material associated with it. A Relative Ionization Efficiency (RIE) of 0.2 (based on calibration with regal black particles) was applied to the rBC data. A CE of 0.6 was applied to all the SP-AMS data (refractory and non-refractory components) based on comparison of SP-AMS rBC and MAAP BC. Laser alignment issues did not allow measurement of aerosol non-refractory components (i.e. black carbon) before 17 November at 19:30 and between 21 November at 19:00 and 23 November at 16:00. The size distribution data from SP-AMS were not available.

Other co-located measurements included NH_3 (Wyers et al., 1993), particle number size distribution (OPC monitor, FAI Rome Italy), and daily PM_1 mass concentration by beta attenuation measurements (Swam dual channel monitor, FAI Rome Italy).

2.5 Aerosol optical properties

Optical measurements of light extinction (b_{ext}, Mm^{-1}) and light absorption (b_{abs}, Mm^{-1}) were respectively measured by a Cavity Attenuated Phase Shift Spectrometer particle extinction monitor, CAPS PMex (Kebabian et al., 2007; Massoli et al., 2010) and a particle soot absorption photometer, PSAP (Bond et al., 1999) valid for the single wavelength model. Internal flow meter was calibrated with respect to a primary air flow calibrator (Gilian Gilibrator), the spot size was measured with a micrometer, while the aerosol scattering properties were determined by an integrating nephelometer (Radiance Research single wavelength M903) and considered in the absorption corrections according to Bond et al. (1999). PSAP data measured at filter transmissions < 30 % were rejected according to updated indications from PSAP manufacturer. The nominal CAPS data did not require any further corrections, as they were already corrected for

ACPD
14, 4787–4826, 2014

gas-phase absorption during automatic zeroing procedure and for the effects of dilution of the sample flow by the mirrors' purge flow (Massoli et al., 2010). The CAPS (630 nm) and M903 (539 nm) data were adjusted logarithmically to the PSAP wavelength (573 nm) according to $(b_{abs})_{573} = (b_{abs})_{630}(630/573)^{\alpha}$ where α is the Ångstrøm exponent calculated by best fitting the columnar aerosol optical depth within 440 nm and 870 nm measured with a POM-02L sun-sky multispectral radiometer (Prede Inc.). Then, the particle single scattering albedo at 573 nm (SSA) was calculated as

$$SSA = (b_{ext} - b_{abs})/b_{ext} \quad (1)$$

The CAPS PMex monitors performed measurements with a precision (2 σ) of 1 Mm^{-1} at 1 s time resolution (decreasing to about 0.1 Mm^{-1} for 5 min integration times). The absolute error in the b_{ext} coefficient was 5 % at maximum.

Both HR-TOF-AMS, the SP-AMS, the CAPS and the PSAP were connected to the same isokinetic inlet for particle sampling.

3 Results

3.1 Campaign overview

Figure 2a shows on-line non-refractory PM_1 (NR-PM_1), together with PM_1 time trend and off-line chemically reconstructed $PM_{1.2}$. PM_1 was estimated as the sum of rBC and non-refractory submicron aerosol components, quantified by SP-AMS and HR-TOF-AMS, respectively. $PM_{1.2}$ represents the sum of sulfate, nitrate, ammonium, water soluble organic mass (WSOM) and water insoluble carbon mass (WICM) from the analysis of the first three stages of size segregated Berner impactor. WSOM was calculated from the water soluble organic carbon, using an OM to OC ratio of 1.6, in agreement with elemental analysis of high resolution AMS data. WICM was derived from water insoluble carbon concentration using a conversion factor of 1.1. The concentration of AMS sulfate, nitrate, and ammonium corrected for CE and averaged over

ACPD
14, 4787–4826, 2014

Berner impactor sampling periods were in agreement with off-line measurements. The good agreement between on-line and off-line measurements indicates that sampling artifacts of submicron particles were negligible and confirmed that the CE correction of the on-line AMS data was accurate.

Total PM_1 concentration, whose average was $22 \pm 15\,\mu g\,m^{-3}$ over the entire campaign, varied with fog, with higher PM_1 values when fog was not present. PM_1 concentration averaged $32 \pm 14\,\mu g\,m^{-3}$ under clear conditions ($LWC < 0.08\,g\,L^{-1}$) and $10 \pm 6\,\mu g\,m^{-3}$ in fog ($LWC > 0.08\,g\,L^{-1}$), corresponding to an average decrease of 60 % in mass during fog events. Concentration reduction occurred rapidly in time. Events characterized by a rapid increase in LWC were associated with a decrease in PM_1 in less than 15 min (Fig. 2a).

PM_1 concentration in the range 10–30 $\mu g\,m^{-3}$ was in agreement with previous measurements performed at the same site during winter 2008 (Carbone et al., 2010). These values, especially for out of fog conditions, are higher than the average $PM_{2.5}$ reported for several rural background and urban background sites (Putaud et al., 2010), and higher than the EU target limit of 25 $\mu g\,m^{-3}$ set by the EU Air quality directive for $PM_{2.5}$ (EU/50/2008).

Figure 2b shows the time trend of the submicron chemical components as measured by the HR-TOF-AMS. Submicron mass was dominated by organics and ammonium nitrate, as observed also in previous campaigns (Carbone et al., 2010). Average mass fraction was 54 ± 12 % for organic matter, 27 ± 10 % for nitrate, 10 ± 3 % for ammonium, and 6 ± 3 % for sulfate.

Previous work showed that the OA loadings in the rural Po Valley during the fall season are usually dominated by traffic emissions and wood burning for residential heating purposes (Gilardoni et al., 2011). To identify OA main sources during fall 2011 in San Pietro Capofiume, PMF analyses were performed on the organic mass spectral matrices. For this database, we chose a 4-factor solution with rotational forcing parameter $f_{Peak} = 0$ ($Q/Q_{exp} = 4$), yielding a hydrocarbon-like OA (HOA) component, a low volatility oxygenated OA (LVOOA) component, and two biomass burning OA (BBOA)

ACPD
14, 4787–4826, 2014

components, which were recombined into one BBOA factor. A detailed summary of key diagnostic plots of the PMF results and a discussion of the factor solution choices are reported in Supplement (Figs. 1S, 2S, 3S, 4S and related text). Figure 3 shows HOA, LVOOA and BBOA from top to bottom. During the campaign the HOA had an average mass of 2 $\mu g\,m^{-3}$, whereas the BBOA was low (0.5 $\mu g\,m^{-3}$) until 22 November and then increased significantly during the rest of the campaign, due to a decrease of ambient temperature and probably increase in emissions from wood burning for residential heating. After 22 November BBOA averaged 2.5 $\mu g\,m^{-3}$, except for a 8 h event occurring between 28 and 29 November, when 16 $\mu g\,m^{-3}$ of BBOA were measured. The LVOOA time series show a more regular pattern through the 2 weeks time period, with loadings going from 1 $\mu g\,m^{-3}$ at night to 5 $\mu g\,m^{-3}$ during the day, thereby following a time trend opposite to that of LWC. In fact the highest concentrations of LVOOA were observed when LWC was lower, i.e. out of fog. Interpretation of PMF factors is more clear when looking at the diurnal profiles of the three factors (Fig. 3), which show a strong diurnal cycle in LVOAA (peaking between 12:00 and 17:00 LT) and a mild opposite trend in the HOA factor (slightly lower during daytime than at night-time). The BBOA diurnal trend is instead mostly flat, due to efficient fog removal during night-time, when higher emissions are expected.

Table 1 summarizes the Pearson correlation coefficients (r) between the three PMF factors and several gas-phase and particle tracers. HOA correlates best with NO (r = 0.62) whereas BBOA correlates with rBC (r = 0.75) and biomass burning tracers, i.e. levoglucosan (r = 0.71) and potassium (r = 0.80). The LVOOA factor correlates strongly with secondary inorganic ions, i.e. sulfate and nitrate (r = 0.85 and r = 0.90, respectively), and has a stronger correlation than BBOA with more oxidized species as oxalic acid (r = 0.96). The LVOOA correlates also with amines, calculated as the sum of monomethyl, dimethyl, and trimethyl amines from off-line HNMR analysis (r = 0.71).

The elemental composition (H/C, O/C, N/C) and the OM/OC calculated using the standard AMS data analysis code (Aiken et al., 2007) are also reported in Fig. 3. The average O/C ratio calculated for the HOA component (0.19) is slightly higher than

ACPD
14, 4787–4826, 2014

what was found for HOA factors of HR-TOF-AMS spectra in urban areas (0.1 or less). However, a very similar HOA mass spectrum (with a fairly large CO_2^+ signal at m/z = 44) was measured during the 2008 spring campaign at the same location (Saarikoski et al., 2012). The relatively large oxygenation for this HOA is likely due to the fact that the SPC station is a rural area away from direct urban and fresher (less oxidized) emissions. The average H/C and O/C values for the BBOA component are 1.59 and 0.24, respectively, consistently with literature BBOA mass spectra (Mohr et al., 2012; Saarikoski et al., 2012). The average H/C and O/C values for the LVOOA component are 1.29 and 0.62, respectively, in agreement with values reported by Ng et al. (2010) for urban downwind and rural areas.

3.2 Fog scavenging

Figure 4 compares the size resolved reconstructed mass and particle composition in the range 50 nm–10 µm during night and day. Data are obtained from off-line analysis of Berner impactor samples, collected during day and night-time. Most of the night-time collection periods overlapped with fog events, so night-time data are representative of in-fog conditions, while daytime average composition represents of out-of-fog conditions.

Aerosol mass concentration of particles smaller than 140 nm and larger than 3.5 µm accounted for less than 10 % of aerosol loading, and was not affected by fog scavenging. Particles with aerodynamic diameter between 140 nm and 1.2 µm were those mostly affected by fog presence. Fog scavenging removed 50 to 70 % of their mass. Occasionally mass concentration of particles larger than 3.5 µm slightly increased during fog, likely due to the collection of fog droplets on the upper impactor stages, as also observed during previous campaigns (Fuzzi et al., 1992).

Comparison of size resolved composition shows that fog scavenging removes water soluble inorganic species more efficiently than organic matter, increasing the contribution of carbonaceous material up to 80–90 % in interstitial particles. In addition, scavenging changes the properties of this carbonaceous fraction increasing the WICM

ACPD
14, 4787–4826, 2014

to WSOM ratio in submicron particles from 0.2–0.3 before fog to 0.6–0.8 during fog. The enrichment of OA in insoluble species is consistent with the results reported by Facchini et al. (1999a) based on fog and interstitial aerosol chemical characterization.

The effect of scavenging on the size and chemical composition of the submicron aerosol was further analyzed with higher resolution using the on-line pTOF measurements from the HR-TOF-AMS (Fig. 5). The figure shows that the mean mode diameter shifted from 300–400 nm to 200–250 nm D_{va} when going from out-of-fog to in-fog conditions. The largest change in mass was observed for nitrate, followed by organics. It is also interesting to see that organic and inorganic components were partially internally mixed (organic modes peaking at slightly smaller D_{va}) both in fog and out of fog.

Table 2 reports mass scavenging efficiency of major chemical components of submicron particles. Based on the HR-TOF-AMS measurements, mass scavenging efficiency (η) was calculated comparing the concentration of each chemical species before fog formation and right after fog formation, according to Noone et al. (1992).

$$\eta = 1 - \frac{[X]\ \text{interstitial}}{[X]\ \text{before fog}} \quad (2)$$

The variability of scavenging efficiency among the different chemical species can be explained by their water solubility. Nitrate and ammonium showed the highest mass scavenging efficiencies, on average 71 and 68 %, respectively. Black carbon, the most hydrophobic component, was the species least efficiently scavenged (39 % on average). OA showed the largest variability, with η ranging between 20 and 60 %, in agreement with previous observations (Collett et al., 2008). Collett et al. (2008) observed a slight correlation between OA scavenging and LWC. During the Po Valley experiment, the variability of η observed among the different fog events could not be explained by the variability of LWC. In fact, the correlation coefficient (r^2) of organic η and LWC was 0.02, indicating that LWC explained only 2 % of the organic scavenging variability.

Fog scavenging of different aerosol chemical components was previously investigated in the Po Valley fog system by Hallberg et al. (1992) and by Facchini et al.

ACPD
14, 4787–4826, 2014

(1999a). The average scavenging efficiencies reported by Hallberg et al. (1992) for sulfate (18 %) and EC (6 %) were significantly lower than those measured during the present study. On the other hand, sulfate scavenging observed at the same site during a different experiment was 60 % (Facchini et al., 1999a) and agrees well with the values here reported. The scavenging efficiencies of ammonium and nitrate measured during the fall 2011 experiment are comparable to the upper bound of the variability range reported by Facchini et al. (1999a) (0.3–0.7). In addition, Facchini et al. (1999a) observed that scavenging of OA was lower compared to that of inorganic species, nevertheless, scavenging of WSOM was similar to that of nitrate and ammonium. The results of the present study confirm those observations and the similarity of nitrate and organic oxygen scavenging suggests that oxygenated organic aerosol could be a proxy for water soluble OA.

Previous scavenging studies lack information about the size distribution of different chemical components, which, together with water solubility, might have a significant role in determining the overall scavenging variability. Scavenging follows particle activation by water uptake, and based on Kohler theory, activation of particles larger than 300–400 nm is more likely to occur than for smaller particles, especially at low supersaturation typical of fog events. Ammonium and nitrate mass size distribution peaked around 400–500 nm D_{va}, organic distribution had a maximum above 250 nm D_{va}, while rBC, whose size distribution was not measured, is expected to peak around 100 nm D_{va} ("primary soot" mode); a much less intense rBC mode can be sometimes present in the accumulation region at 400–450 nm D_{va} ("aged soot" mode) for aged aerosol (Onasch et al., 2012; Massoli et al., 2012).

Figure 6 shows the trends in single scattering albedo (SSA) obtained from combining CAPS extinction and PSAP absorption coefficients. The SSA shows a diurnal trend with high SSA values during the day without fog (reaching 0.9 during midday) and low SSA values at night in fog, with SSA values as low as 0.7. This is consistent with the time trends shown in Figs. 2 and 3 and with the fact that fog scavenging removed water-soluble species (hygroscopic and light scattering) and left behind particles enriched

ACPD
14, 4787–4826, 2014

in carbonaceous material (less hygroscopic and more light-absorbing). The smoother diurnal trend in SSA observed between 21 and 25 November corresponds to times when the fog events were less pronounced, LWC was low and temperature was varying less (cf. Figs. 1 and 2).

4 Discussion

The objective of this section is to investigate the effect of particle composition and microphysical properties on nucleation scavenging. Eq. (2) assumes that the same air parcel is sampled before and right after fog formation; intrusion of new air masses would change the composition of aerosol, making nucleation scavenging calculation inaccurate. For this reason, (i) we calculated scavenging efficiency based on observations over a short time interval (30 min before and after fog formation) and (ii) we excluded fog events associated with fog transport or intrusion. The time interval of 30 min was chosen as the shortest interval that allowed an accurate pTOF measurement. Intrusion events were identified based on the analysis of meteorological parameters (Table 2).

Fog events 2, 3, 4, 5, 6, 8, 9, 10, 12, and 13 were characterized by temperature decrease, stagnant conditions (i.e. wind speed below $2\,m\,s^{-1}$), and almost complete scavenging of particle above 700 nm. In agreement with previous observations in the Po Valley we classified these events as radiation fog (Noone et al., 1992; Wobrock et al., 1992; Whiteaker et al., 2002). Thus, changes in aerosol concentration should be attributed mainly to nucleation scavenging. On the contrary, we identified as fog transport/intrusion events (1, 7, 11, and 14) those characterized by null or very small temperature variation and higher wind speed. The scavenging of particles larger than 700 nm was consistently below 70 % (Table 2).

To study the effect of chemical composition and particle size on scavenging, we investigated scavenging efficiency size distribution for the main submicron chemical components: nitrate, as representative of inorganic aerosol, and organics.

ACPD
14, 4787–4826, 2014

4.1 Nitrate scavenging

Figure 7a reports the size distribution of η for nitrate mass concentration corresponding to the different radiation fog events. η is calculated comparing nitrate size distribution from pTOF measurements averaged over 30 min before fog formation and over 30 min after fog formation. Other than event 4 and 9, all fog events showed similar variation of η, with values of about 0.5 at 200 nm D_{va}, corresponding to a geometric diameter of 133 nm (assuming spherical particles with density 1.5 g cm^{-3}).

The largest variation of η was observed below 200 nm (from 20 % to 80 %), while above 400 nm η ranged between 90 and 100 % for all the events. We explained η variability based on particle chemical composition, particularly by taking into account the contribution of organic matter to particle mass. While ammonium nitrate is water soluble and ammonium nitrate particles are hydrophylic, organics are less water soluble and organic particulate matter is expected to be more hydrophobic (Petters and Kreidenweis, 2008). Figure 8a shows that η of nitrate was higher for larger particles and smaller for smaller particles. Within the same size range, η decreased with increasing organic mass fraction, i.e. increasing the contribution of a more hydrophobic component. Similarly, Fig. 8b reports η variability as a function of κ (Petters and Kreidenweis, 2008). κ is a measure of particle hygroscopicity, and was calculated assuming that aerosol was internally mixed, according to:

$$\kappa = \sum_i \epsilon_i \kappa_i \quad (3)$$

ϵ_i and κ_i are the volume fraction and the hygroscopicity of the single component i, respectively. To calculate the volume fractions, the following densities were used: 1.72 g cm^{-3} for nitrate, 1.78 g cm^{-3} for sulfate, 1.75 g cm^{-3} for ammonium, 1.4 g cm^{-3} for chloride, and 1.27 g cm^{-3} for organics (Duplissy et al., 2011). κ_i was assumed equal to 0.7 for nitrate, sulfate, and ammonium, 1.3 for chloride, and 0.15 for organics (Petters and Kreidenweis, 2007; Jimenez et al., 2009; Gunthe et al., 2009; Chang et al., 2010).

ACPD
14, 4787–4826, 2014

Within each size range, more hygroscopic particles were more efficiently scavenged. The hygroscopicity had a larger effect on η of smaller particles, while for particles larger than 300 nm hygroscopicity, and thus chemical composition, affected scavenging weakly. The correlation coefficients r^2 corresponding to particles below 200 nm D_{va} (0.51) indicates that hygroscopicity explained 50 % of nitrate scavenging variability.

4.2 Organic scavenging

Figure 7b reports the size distribution of η for organic mass concentration. η curves for organics are slightly lower than nitrate curves (average nitrate is reported in black) and showed a larger variability. η for organics reached 0.5 around 250 nm D_{va}, and increased with increasing diameter, reaching values above 0.9 only for particles larger than 600 nm D_{va}. Event 2 is not reported because the organic loading was too low to allow an accurate analysis of scavenging size trend.

The similarity between organic and nitrate η curves supports the hypothesis that most of the organic mass was internally mixed with nitrate, as also suggested by the similar size distribution of pTOFs curves (Fig. 5). In fact, if organics were not internally mixed with water soluble species, their scavenging below 1 µm at very low supersaturation observed in fog would be close to zero (Petters and Kreidenweis, 2008). It follows that the largest part of organic mass scavenged in submicron particles was internally mixed with nitrate. Based on this conclusion we can estimate the organic mass fraction internally mixed with nitrate as the average organic to nitrate scavenging ratio. In the range 150–700 nm, 50 to 90 % of organic mass was internally mixed with nitrate. The lower mixing ratios were observed for particles smaller than 200 nm D_{va}, on average 35 %, in agreement with values expected for primary and less processed particles.

OA composition was further investigated by FTIR spectroscopy. To verify the consistency between AMS and FTIR results, we compared the oxygen to carbon ratio (O/C), estimated by elemental analysis of AMS data (Aiken et al., 2008) to the one calculated by the contribution of oxygenated and not oxygenated functional groups quantified by FTIR spectroscopy. Among oxygenated groups, FTIR identified organonitrates, which

ACPD
14, 4787–4826, 2014

are not included in the organic oxygen budget in the AMS analysis. Thus, we compared the O/C ratio from AMS to the FTIR ratio calculated without the contribution of organonitrates. Figure 9 shows that the agreement between the two techniques was satisfactory (generally within 10 %) for samples characterized by shorter collection period (below 15 h) (Maria et al., 2003). In the following paragraphs we limit our considerations to those samples characterized by a collection period shorter than 15 h.

Functional group analysis by FTIR showed that organic mass was mainly composed of alkylic, carboxylic, and hydroxyl groups, representing on average 44 %, 28 %, and 22 % of organic mass, respectively. Organic nitrogen species, i.e. amines and organonitrates, accounted for a small fraction of the OA loading.

It is worth noting that the organonitrate functional group represents a small fraction of organic mass, nevertheless its presence could affect the O/C ratio. For example, when organic-nitrates composed 6 % of organic mass, the O/C ratio was 14 % higher than the O/C measured by AMS or calculated by FTIR functional group excluding nitrate contribution.

Table 3 reports the scavenging efficiency of organic aerosol for four fog events, when organic functional group composition from FTIR was available right before fog formation. The scavenging efficiency of organic aerosol was slightly correlated with the average oxidation state of organic carbon (OS_c), calculated according to Kroll et al. (2011) and based on FTIR data. Samples characterized by the highest O/C ratio and the lowest OS_c were also associated with the highest organic aerosol scavenging (18 and 28 November). The higher scavenging of more oxidized aerosol is also confirmed by higher scavenging efficiency of organic oxygen compared to organic aerosol as total (Table 2). This result can be attributed to the highest polarity, and thus solubility, of oxidized organic aerosols and to a more efficient mixing of oxidized/aged organics with secondary inorganic aerosol, which is more hydrophilic.

We speculate that the effect of mixing might be more relevant than the effect of polarity and solubility by itself. If oxidized organics were removed by fog more efficiently than less oxidized species only because more soluble, then the scavenging of organic

ACPD
14, 4787–4826, 2014

oxygen should have been constant or only slightly variable, as observed for example for nitrate. The fact that organic oxygen scavenging efficiency varied by 18 percentage points, during radiation fog events, indicates that a different effect is controlling its scavenging, more likely efficiency of mixing with water soluble species.

This conclusion is further supported by the analysis of the main oxygenated organic functional groups. Table 3 reports the molar ratio of the carboxylic (COOH) to the hydroxyl (OH) group. COOH and OH groups are expected to affect solubility in different ways. In fact, COOH group has a dipole moment larger than OH group, thus given a certain carbon skeleton molecule, the COOH group would increase its solubility more than a OH group. The fog events of 28, 29, and 30 November showed a very similar COOH to OH ratio, indicating that the relative contribution of oxygenated functional groups was similar. Nevertheless, organic oxygen scavenging efficiency varied from 57 to 75 %. This result suggests that the chemical nature of organic oxygen, which should control OA polarity and solubility, could not explain the variability in organic oxygen scavenging that was observed during the Po Valley experiment.

5 Conclusions

The employment of high time resolution techniques allowed the investigation of chemical and microphysical properties of fine particles immediately before and after fog formation, during 14 distinct fog events.

The highest scavenging efficiencies were observed for nitrate, ammonium, and sulfate, respectively 70 %, 68 %, and 61 %. Scavenging of organic aerosol averaged 50 %, while the lowest values characterized black carbon (39 % on average).

Fog removed preferentially water-soluble components and oxidized organic aerosol in particle with vacuum aerodynamic dry diameter larger than 400 nm, leaving an interstitial aerosol enriched in water insoluble and less oxidized carbonaceous species.

Although scavenging of water soluble species, like nitrate, was close to completeness above 400 nm D_{va}, it was strongly affected by chemical composition in smaller

ACPD
14, 4787–4826, 2014

size ranges, especially when less water soluble species, like OA, were present. These results indicate that at very high relative humidity, OA affects significantly particle ability to uptake water and form droplets. This implies that models require an accurate description of particle microphysics in order to describe both particle wet removal and atmospheric processing through heterogenous phase chemistry.

Nucleation scavenging of OA varied between 45 % and 63 %. A slight correlation between OS_c and scavenging efficiency was observed. Nevertheless, the correlation of size segregated scavenging efficiency with that of nitrate, and the similarity of nitrate and OA size distributions before and after fog formation, suggest that organic scavenging was controlled by mixing with water soluble inorganic species. The small variability of the degree of oxidation of OA and functional group composition during the experiment made impossible to discriminate the role of OA composition on its scavenging.

To summarize, fog represents a significant sink of pollutants on a regional scale, especially in highly polluted areas characterized by cold winter and stagnant atmospheric conditions, like the Po Valley. Here we have shown that scavenging is very efficient for nitrate and inefficient for BC. Scavenging of organic component is highly variable, and further studies are required to distinguish particle-mixture effects from organic composition effects.

Supplementary material related to this article is available online at http://www.atmos-chem-phys-discuss.net/14/4787/2014/acpd-14-4787-2014-supplement.pdf.

Acknowledgements. This research was funded by Regione Emilia Romagna as part of the "Supersito" Project (DRG n. 428/10). The authors acknowledge L. Tarozzi and C. Carbone for their support during aerosol sampling activity, M. R. Canagaratna for her support during PMF analysis, and A. Freedman for providing the CAPS-PM measurement data.

ACPD
14, 4787–4826, 2014

References

Bond, T. C., Anderson, T. L., and Campbell, D.: Calibration and intercomparison of filter-based measurements of visible light absorption by aerosols, Aerosol Sci. Tech., 30, 582–600, 1999. 4795

Carbone, C., Decesari, S., Mircea, M., Giulianelli, L., Finessi, E., Rinaldi, M., Fuzzi, S., Marinoni, A., Duchi, R., Perrino, C., Sargolini, T., Vardè, M., Sprovieri, F., Gobbi, G. P., Angelini, F., and Facchini, M. C.: Size-resolved aerosol chemical composition over the Italian Peninsula during typical summer and winter conditions, Atmos. Environ., 44, 5269–5278, 2010. 4797

Chang, R. Y.-W., Slowik, J. G., Shantz, N. C., Vlasenko, A., Liggio, J., Sjostedt, S. J., Leaitch, W. R., and Abbatt, J. P. D.: The hygroscopicity parameter (κ) of ambient organic aerosol at a field site subject to biogenic and anthropogenic influences: relationship to degree of aerosol oxidation, Atmos. Chem. Phys., 10, 5047–5064, doi:10.5194/acp-10-5047-2010, 2010. 4803

Collett Jr., J. L., Sherman, D. E., Moore, K., Hannigan, M., and Lee, T.: Aerosol Particle Processing and Removal by Fogs: Observations in Chemically Heterogeneous Central California Radiation Fogs, Water Air Soil Poll.-Focus, 1, 303–312, 2001. 4789

Collett, J. L., Herckes, P., Youngster, S., and Lee, T.: Processing of atmospheric organic matter by California radiation fogs, Atmos. Res., 87, 232–241, 2008. 4789, 4790, 4800

DeCarlo, P. F., Kimmel, J. R., Trimborn, A., Northway, M. J., Jayne, J. T., Aiken, A. C., Gonin, M., Fuhrer, K., Horvath, T., Docherty, K. S., Worsnop, D. R., and Jimenez, J. L.: Field-deployable, high-resolution, time-of-flight aerosol mass spectrometer, Anal. Chem., 78, 8281–8289, 2006. 4794

Decesari, S., Fuzzi, S., Facchini, M. C., Mircea, M., Emblico, L., Cavalli, F., Maenhaut, W., Chi, X., Schkolnik, G., Falkovich, A., Rudich, Y., Claeys, M., Pashynska, V., Vas, G., Kourtchev, I., Vermeylen, R., Hoffer, A., Andreae, M. O., Tagliavini, E., Moretti, F., and Artaxo, P.: Characterization of the organic composition of aerosols from Rondônia, Brazil, during the LBA-SMOCC 2002 experiment and its representation through model compounds, Atmos. Chem. Phys., 6, 375–402, doi:10.5194/acp-6-375-2006, 2006. 4793

Duplissy, J., DeCarlo, P. F., Dommen, J., Alfarra, M. R., Metzger, A., Barmpadimos, I., Prevot, A. S. H., Weingartner, E., Tritscher, T., Gysel, M., Aiken, A. C., Jimenez, J. L., Canagaratna, M. R., Worsnop, D. R., Collins, D. R., Tomlinson, J., and Baltensperger, U.: Relating

ACPD
14, 4787–4826, 2014

hygroscopicity and composition of organic aerosol particulate matter, Atmos. Chem. Phys., 11, 1155–1165, doi:10.5194/acp-11-1155-2011, 2011. 4803

Dusek, U., Frank, G. P., Hildebrandt, L., Curtius, J., Schneider, J., Walter, S., Chand, D., Drewnick, F., Hings, S., Jung, D., Borrmann, S., and Andreae, M. O.: Size matters more than chemistry for cloud-nucleating ability of aerosol particles, Science, 312, 1375–1378, 2006. 4790

Elbert, W., Hoffmann, M. R., Krämer, M., Schmitt, G., and Andreae, M. O.: Control of solute concentrations in cloud and fog water by liquid water content, Atmos. Environ., 34, 1109–1122, 2000. 4789, 4790

Ervens, B., Turpin, B. J., and Weber, R. J.: Secondary organic aerosol formation in cloud droplets and aqueous particles (aqSOA): a review of laboratory, field and model studies, Atmos. Chem. Phys., 11, 11069–11102, doi:10.5194/acp-11-11069-2011, 2011. 4789

Facchini, M. C., Fuzzi, S., Zappoli, S., Andracchio, A., Gelencsér, A., Kiss, G., Krivácsy, Z., Mészáros, E., Hansson, H.-C., Alsberg, T., and Zebühr, Y.: Partitioning of the organic aerosol component between fog droplets and interstitial air, J. Geophys. Res.-Atmos., 104, 26821–26832, 1999a. 4790, 4800, 4801

Facchini, M. C., Mircea, M., Fuzzi, S., and Charlson, R. J.: Cloud albedo enhancement by surface-active organic solutes in growing droplets, Nature, 401, 257–259, 1999b. 4790

Fuzzi, S., Orsi, G., Nardini, G., Facchini, M. C., McLaren, S., McLaren, E., and Mariotti, M.: Heterogeneous processes in the Po Valley radiation fog, J. Geophys. Res.-Atmos., 93, 11141–11151, 1988. 4789

Fuzzi, S., Facchini, M. C., Orsi, G., Lind, J. A., Wobrock, W., Kessel, M., Maser, R., Jaeschke, W., Enderle, K. H., Arends, B. G., Berner, A., Solly, I., Kruisz, C., Reischl, G., Pahl, S., Kaminski, U., Winkler, P., Ogren, J. A., Noone, K. J., Hallberg, A., Fierlinger-Oberlinninger, H., Puxbaum, H., Marzorati, A., Hansson, H. C., Wiedensohler, A., Svenningsson, I. B., Martinsson, B. G., Schell, D., and Gerogii, H. W.: The Po Valley fog experiment 1989, Tellus B, 44, 448–468, 1992. 4791, 4799

Gerber, H.: Direct measurement of suspended particulate volume concentration and far-infrared extinction coefficient with a laser-diffraction instrument, Appl. Optics, 30, 4824–4831, 1991. 4792

Gilardoni, S., Liu, S., Takahama, S., Russell, L. M., Allan, J. D., Steinbrecher, R., Jimenez, J. L., De Carlo, P. F., Dunlea, E. J., and Baumgardner, D.: Characterization of organic ambi-

ACPD
14, 4787–4826, 2014

ent aerosol during MIRAGE 2006 on three platforms, Atmos. Chem. Phys., 9, 5417–5432, doi:10.5194/acp-9-5417-2009, 2009. 4793
Gilardoni, S., Vignati, E., Cavalli, F., Putaud, J. P., Larsen, B. R., Karl, M., Stenström, K., Genberg, J., Henne, S., and Dentener, F.: Better constraints on sources of carbonaceous aerosols using a combined $_{14}C$ – macro tracer analysis in a European rural background site, Atmos. Chem. Phys., 11, 5685–5700, doi:10.5194/acp-11-5685-2011, 2011. 4797
Gunthe, S. S., King, S. M., Rose, D., Chen, Q., Roldin, P., Farmer, D. K., Jimenez, J. L., Artaxo, P., Andreae, M. O., Martin, S. T., and Pöschl, U.: Cloud condensation nuclei in pristine tropical rainforest air of Amazonia: size-resolved measurements and modeling of atmospheric aerosol composition and CCN activity, Atmos. Chem. Phys., 9, 7551–7575, doi:10.5194/acp-9-7551-2009, 2009. 4803
Hallberg, A., Ogren, J. A., Noone, K. J., Heintzenberg, J., Berner, A., Solly, I., Kruisz, C., Reischl, G., Fuzzi, S., Facchini, M. C., Hansson, H. C., Wiedensohler, A., and Svenningsson, I. B.: Phase partitioning for different aerosol species in fog, Tellus B, 44, 545–555, 1992. 4789, 4800, 4801
Herckes, P., Chang, H., Lee, T., and Collett, Jeffrey, L., J.: Air Pollution Processing by Radiation Fogs, Water Air Soil Pollut., 181, 65–75, 2007. 4790
Hudson, J. G.: Variability of the relationship between particle size and cloud-nucleating ability, Geophys. Res. Lett., 34, 2007. 4790
Jimenez, J. L., Jayne, J. T., Shi, Q., Kolb, C. E., Worsnop, D. R., Yourshaw, I., Seinfeld, J. H., Flagan, R. C., Zhang, X., Smith, K. A., Morris, J. W., and Davidovits, P.: Ambient aerosol sampling using the Aerodyne Aerosol Mass Spectrometer, J. Geophys. Res.-Atmos., 108, 8425, doi:10.1029/2001JD001213, 2003. 4794
Jimenez, J. L., Canagaratna, M. R., Donahue, N. M., Prevot, A. S. H., Zhang, Q., Kroll, J. H., DeCarlo, P. F., Allan, J. D., Coe, H., Ng, N. L., Aiken, A. C., Docherty, K. S., Ulbrich, I. M., Grieshop, A. P., Robinson, A. L., Duplissy, J., Smith, J. D., Wilson, K. R., Lanz, V. A., Hueglin, C., Sun, Y. L., Tian, J., Laaksonen, A., Raatikainen, T., Rautiainen, J., Vaattovaara, P., Ehn, M., Kulmala, M., Tomlinson, J. M., Collins, D. R., Cubison, M. J., E., Dunlea, J., Huffman, J. A., Onasch, T. B., Alfarra, M. R., Williams, P. I., Bower, K., Kondo, Y., Schneider, J., Drewnick, F., Borrmann, S., Weimer, S., Demerjian, K., Salcedo, D., Cottrell, L., Griffin, R., Takami, A., Miyoshi, T., Hatakeyama, S., Shimono, A., Sun, J. Y., Zhang, Y. M., Dzepina, K., Kimmel, J. R., Sueper, D., Jayne, J. T., Herndon, S. C., Trimborn, A. M., Williams, L. R., Wood, E. C., Middlebrook, A. M., Kolb, C. E., Baltensperger, U.,

ACPD
14, 4787–4826, 2014

and Worsnop, D. R.: Evolution of organic aerosols in the atmosphere, Science, 326, 1525–1529, 2009. 4803
Kaul, D. S., Gupta, T., Tripathi, S. N., Tare, V., and Collett, J. L.: Secondary organic aerosol: a comparison between foggy and nonfoggy days, Environ. Sci. Technol., 45, 7307–7313, 2011. 4789
Kebabian, P. L., Robinson, W. A., and Freedman, A.: Optical extinction monitor using cw cavity enhanced detection, Rev. Sci. Instrum., 78, 063102, doi:10.1063/1.2744223, 2007. 4795
Kroll, J. H., Donahue, N. M., Jimenez, J. L., Kessler, S. H., Canagaratna, M. R., Wilson, K. R., Altieri, K. E., Mazzoleni, L. R., Wozniak, A. S., Bluhm, H., Mysak, E. R., Smith, J. D., Kolb, C. E., and Worsnop, D. R.: Carbon oxidation state as a metric for describing the chemistry of atmospheric organic aerosol, Nature Chemistry, 3, 133–139, 2011. 4805
Laaksonen, A., Korhonen, P., Kulmala, M., and Charlson, R. J.: Modification of the Köhler Equation to Include Soluble Trace Gases and Slightly Soluble Substances, J. Atmos. Sci., 55, 853–862, 1998. 4790
Levin, E. J. T., Prenni, A. J., Palm, B., Day, D., Campuzano-Jost, P., Winkler, P. M., Kreidenweis, S. M., DeMott, P. J., Jimenez, J., and Smith, J. N.: Size-resolved aerosol composition and link to hygroscopicity at a forested site in Colorado, Atmos. Chem. Phys. Discuss., 13, 23817–23843, doi:10.5194/acpd-13-23817-2013, 2013. 4790
Li, Y. J., Lee, B. Y. L., Yu, J. Z., Ng, N. L., and Chan, C. K.: Evaluating the degree of oxygenation of organic aerosol during foggy and hazy days in Hong Kong using high-resolution time-of-flight aerosol mass spectrometry (HR-ToF-AMS), Atmos. Chem. Phys., 13, 8739–8753, doi:10.5194/acp-13-8739-2013, 2013. 4789
Liu, P. S. K., Deng, R., Smith, K. A., Williams, L. R., Jayne, J. T., Canagaratna, M. R., Moore, K., Onasch, T. B., Worsnop, D. R., and Deshler, T.: Transmission efficiency of an aerodynamic focusing lens system: comparison of model calculations and laboratory measurements for the Aerodyne Aerosol Mass Spectrometer, Aerosol Sci. Tech., 41, 721–733, 2007. 4794
Maria, S. F. and Russell, L. M.: Organic and inorganic aerosol below-cloud scavenging by suburban New Jersey precipitation, Environ. Sci. Technol., 39, 4793–4800, 2005. 4790
Maria, S. F., Russell, L. M., Turpin, B. J., Porcja, R. J., Campos, T. L., Weber, R. J., and Huebert, B. J.: Source signatures of carbon monoxide and organic functional groups in Asian Pacific regional Aerosol Characterization Experiment (ACE-Asia) submicron aerosol types, J. Geophys. Res.-Atmos., 108, 8637, doi:10.1029/2003JD003703, 2003. 4805

ACPD
14, 4787–4826, 2014

Massoli, P., Kebabian, P. L., Onasch, T. B., Hills, F. B., and Freedman, A.: Aerosol light extinction measurements by Cavity Attenuated Phase Shift (CAPS) spectroscopy: laboratory validation and field deployment of a compact aerosol particle extinction monitor, Aerosol Sci. Tech., 44, 428–435, 2010. 4795, 4796

Massoli, P., Fortner, E. C., Canagaratna, M. R., Williams, L. R., Zhang, Q., Sun, Y., Schwab, J. J., Trimborn, A., Onasch, T. B., Demerjian, K. L., Kolb, C. E., Worsnop, D. R., and Jayne, J. T.: Pollution gradients and chemical characterization of particulate matter from vehicular traffic near major roadways: results from the 2009 Queens College air quality study in NYC, Aerosol Sci. Tech., 46, 1201–1218, doi:10.1080/02786826.2012.701784, 2012. 4801

Middlebrook, A. M., Bahreini, R., Jimenez, J. L., and Canagaratna, M. R.: Evaluation of composition-dependent collection efficiencies for the Aerodyne Aerosol Mass Spectrometer using field data, Aerosol Sci. Tech., 46, 258–271, 2011. 4794

Ming, Y. and Russell, L. M.: Organic aerosol effects on fog droplet spectra, J. Geophys. Res.-Atmos., 109, D10206, doi:10.1029/2003JD004427, 2004. 4790

Mohr, C., DeCarlo, P. F., Heringa, M. F., Chirico, R., Slowik, J. G., Richter, R., Reche, C., Alastuey, A., Querol, X., Seco, R., Peñuelas, J., Jiménez, J. L., Crippa, M., Zimmermann, R., Baltensperger, U., and Prévôt, A. S. H.: Identification and quantification of organic aerosol from cooking and other sources in Barcelona using aerosol mass spectrometer data, Atmos. Chem. Phys., 12, 1649–1665, doi:10.5194/acp-12-1649-2012, 2012. 4799

Ng, N. L., Canagaratna, M. R., Zhang, Q., Jimenez, J. L., Tian, J., Ulbrich, I. M., Kroll, J. H., Docherty, K. S., Chhabra, P. S., Bahreini, R., Murphy, S. M., Seinfeld, J. H., Hildebrandt, L., Donahue, N. M., DeCarlo, P. F., Lanz, V. A., Prévôt, A. S. H., Dinar, E., Rudich, Y., and Worsnop, D. R.: Organic aerosol components observed in Northern Hemispheric datasets from Aerosol Mass Spectrometry, Atmos. Chem. Phys., 10, 4625–4641, doi:10.5194/acp-10-4625-2010, 2010. 4799

Noone, K. J., Ogren, J. A., Hallberg, A., Heintzenberg, J., Strom, J., Hansson, H.-C., Svenningsson, B., Wiedensohler, A., Fuzzi, S., Facchini, M. C., Arends, B. G., and Berner, A.: Changes in aerosol size- and phase distributions due to physical and chemical processes in fog, Tellus B, 44, 489–504, 1992. 4790, 4800, 4802

Onasch, T. B., Trimborn, A., Fortner, E. C., Jayne, J. T., Kok, G. L., Williams, L. R., Davidovits, P., and Worsnop, D. R.: Soot particle aerosol mass spectrometer: development, validation, and initial application, Aerosol Sci. Tech., 46, 804–817, 2012. 4794, 4801

ACPD
14, 4787–4826, 2014

Paatero, P. and Tapper, U.: Positive matrix factorization: A non-negative factor model with optimal utilization of error estimates of data values, Environmetrics, 5, 111–126, 1994. 4794
Petters, M. D. and Kreidenweis, S. M.: A single parameter representation of hygroscopic growth and cloud condensation nucleus activity, Atmos. Chem. Phys., 7, 1961–1971, doi:10.5194/acp-7-1961-2007, 2007. 4803
Petters, M. D. and Kreidenweis, S. M.: A single parameter representation of hygroscopic growth and cloud condensation nucleus activity – Part 2: Including solubility, Atmos. Chem. Phys., 8, 6273–6279, doi:10.5194/acp-8-6273-2008, 2008. 4803, 4804
Putaud, J. P., Van Dingenen, R., Alastuey, A., Bauer, H., Birmili, W., Cyrys, J., Flentje, H., Fuzzi, S., Gehrig, R., Hansson, H. C., Harrison, R. M., Herrmann, H., Hitzenberger, R., Hüglin, C., Jones, A. M., Kasper-Giebl, A., Kiss, G., Kousa, A., Kuhlbusch, T. A. J., Löschau, G., Maenhaut, W., Molnar, A., Moreno, T., Pekkanen, J., Perrino, C., Pitz, M., Puxbaum, H., Querol, X., Rodriguez, S., Salma, I., Schwarz, J., Smolik, J., Schneider, J., Spindler, G., ten Brink, H., Tursic, J., Viana, M., Wiedensohler, A., and Raes, F.: A European aerosol phenomenology – 3: Physical and chemical characteristics of particulate matter from 60 rural, urban, and kerbside sites across Europe, Atmos. Environ., 44, 1308–1320, 2010. 4797
Quinn, P. K., Bates, T. S., Coffman, D. J., and Covert, D. S.: Influence of particle size and chemistry on the cloud nucleating properties of aerosols, Atmos. Chem. Phys., 8, 1029–1042, doi:10.5194/acp-8-1029-2008, 2008. 4790
Russell, L. M., Takahama, S., Liu, S., Hawkins, L. N., Covert, D. S., Quinn, P. K., and Bates, T. S.: Oxygenated fraction and mass of organic aerosol from direct emission and atmospheric processing measured on the R/V Ronald Brown during TEXAQS/GoMACCS 2006, J. Geophys. Res.-Atmos., 114, 2009. 4793
Russell, L. M., Bahadur, R., and Ziemann, P. J.: Identifying organic aerosol sources by comparing functional group composition in chamber and atmospheric particles, P. Natl. Acad. Sci. USA, 108, 3516–3521, 2011. 4793
Saarikoski, S., Carbone, S., Decesari, S., Giulianelli, L., Angelini, F., Canagaratna, M., Ng, N. L., Trimborn, A., Facchini, M. C., Fuzzi, S., Hillamo, R., and Worsnop, D.: Chemical characterization of springtime submicrometer aerosol in Po Valley, Italy, Atmos. Chem. Phys., 12, 8401–8421, doi:10.5194/acp-12-8401-2012, 2012. 4799
Seinfeld, J. H. and Pandis, S. N.: Atmospheric Chemistry and Physics: from Air Pollution to Climate Change, John Wiley & Sons, Inc., Hoboken, NJ, 1998. 4789

ACPD
14, 4787–4826, 2014

Shulman, M. L., Jacobson, M. C., Carlson, R. J., Synovec, R. E., and Young, T. E.: Dissolution behavior and surface tension effects of organic compounds in nucleating cloud droplets, Geophys. Res. Lett., 23, 277–280, 1996. 4790

Ulbrich, I. M., Canagaratna, M. R., Zhang, Q., Worsnop, D. R., and Jimenez, J. L.: Interpretation of organic components from Positive Matrix Factorization of aerosol mass spectrometric data, Atmos. Chem. Phys., 9, 2891–2918, doi:10.5194/acp-9-2891-2009, 2009. 4794

Whiteaker, J. R., Suess, D. T., and Prather, K. A.: Effects of meteorological conditions on aerosol composition and mixing state in Bakersfield, CA, Environ. Sci. Technol., 36, 2345–2353, 2002. 4802

Wobrock, W., Schell, D., Maser, R., Kessel, M., Jaeschke, W., Fuzzi, S., Facchini, M. C., Orsi, G., Marzorati, A., Winkler, P., Arends, B. G., and Bendix, J.: Meteorological characteristics of the Po Valley fog, Tellus B, 44, 469–488, 1992. 4802

Wyers, G. P., Otjes, R. P., and Slanina, J.: A continuous-flow denuder for the measurement of ambient concentrations and surface-exchange fluxes of ammonia, Atmos. Environ. A, 27, 2085–2090, 1993. 4795

Zhang, Q., Jimenez, J. L., Canagaratna, M. R., Ulbrich, I. M., Ng, N. L., Worsnop, D. R., and Sun, Y.: Understanding atmospheric organic aerosols via factor analysis of aerosol mass spectrometry: a review, Anal. Bioanal. Chem., 10, 3045–3067, 2011. 4794

ACPD
14, 4787–4826, 2014

Table 1. Correlation coefficients *r* of the PMF factors with the main external gas-phase and aerosol tracers measured at SPC during the campaign. The values in bold denote the highest correlations for each factor. The asterisks indicate data from filter analysis.

Species	HOA	BBOA	LVOOA
BC	0.35	**0.75**	0.30
NO	**0.62**	0.34	−0.34
O_3	0.36	−0.06	0.50
Sulfate	−0.03	0.20	**0.85**
Nitrate	−0.05	0.25	**0.90**
Chloride	0.05	0.55	0.48
Levoglucosan*	0.33	**0.71**	0.14
K^{+*}	−0.20	**0.80**	0.49
Oxalic Acid*	−0.47	0.61	**0.96**

ACPD
14, 4787–4826, 2014

Table 2. Mass scavenging efficiency (η) of the different chemical species, scavenging of particle larger than 700 nm ($N > 700$ nm), and meteorological parameters characteristic of each fog event.

					η				Meteorological parameter		
Event	BC	Chl	NH_4	NO_3	Org	SO_4	Org-oxygen	$N > 700$ nm	LWC ($g L^{-1}$)	T drop (°C)	WS ($m s^{-1}$)
1		0.21	0.52	0.56	0.41	0.58	0.51	0.4	0.14	0.0	2.0
2		0.69	0.73	0.74	0.45	0.76	0.60	0.8	0.14	3.1	0.9
3		0.71	0.76	0.78	0.57	0.73	0.65	0.8	0.18	5.9	1.5
4	0.57	0.81	0.78	0.79	0.63	0.81	0.73	0.9	0.20	2.9	1.7
5	0.56	0.90	0.82	0.85	0.61	0.72	0.69	0.7	0.13	1.8	1.0
6	0.40	0.69	0.75	0.75	0.54	0.70	0.66	0.7	0.13	3.1	1.5
7		0.04	0.42	0.47	0.22	0.12	0.29	0.6	0.16	0.5	1.9
8	0.53	0.71	0.77	0.79	0.61	0.78	0.70	0.8	0.18	3.6	1.1
9		0.45	0.74	0.77	0.54	0.57	0.62	0.8	0.21	4.1	1.8
10	0.42	0.81	0.84	0.85	0.56	0.71	0.75	0.8	0.19	4.1	1.2
11		0.49	0.46	0.48	0.37	0.31	0.42	0.7	0.20	1.0	1.9
12	0.31	0.66	0.73	0.74	0.52	0.66	0.62	0.7	0.14	4.4	1.3
13	0.33	0.47	0.70	0.74	0.49	0.50	0.57	0.7	0.11	3.9	1.1
14		0.54	0.56	0.57	0.51	0.50	0.55	–	0.21	−1.5	1.7

ACPD
14, 4787–4826, 2014

Table 3. Comparison of scavenging efficiency of organic aerosol and organic oxygen with elemental analysis and organic functional group data.

Date Event #	18 Nov 11 4	28 Nov 11 10	29 Nov 11 12	30 Nov 11 13
η organic	0.63	0.56	0.52	0.49
η org oxygen	0.73	0.75	0.62	0.57
O/C	0.52	0.50	0.47	0.40
COOH/OH	2.00	0.77	0.80	0.79

ACPD
14, 4787–4826, 2014

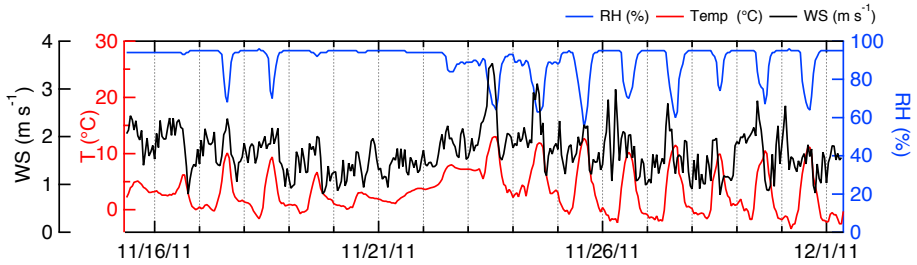

Fig. 1. Time trend of temperature (red), relative humidity (blue), and wind speed (black) at San Pietro Capofiume during the research campaign.

ACPD
14, 4787–4826, 2014

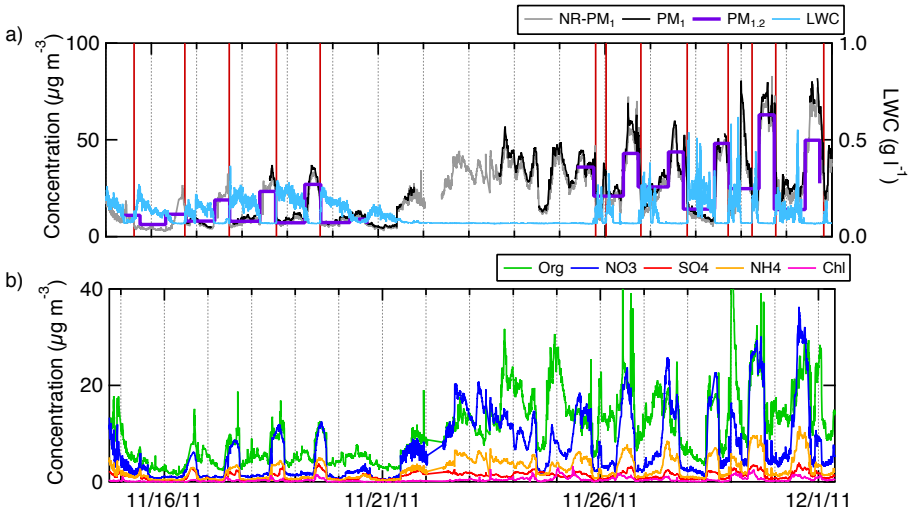

Fig. 2. (a) Time trend of liquid water content (light blue), non refractory PM_1 (grey), PM_1 (purple), and chemically reconstructed $PM_{1,2}$ from off-line analysis (thick black); red vertical lines identify the beginning of fog events. **(b)** Time trend of chemical species from AMS analysis: organics (green), nitrate (blue), sulfate (red), ammonium (orange), chloride (pink).

ACPD
14, 4787–4826, 2014

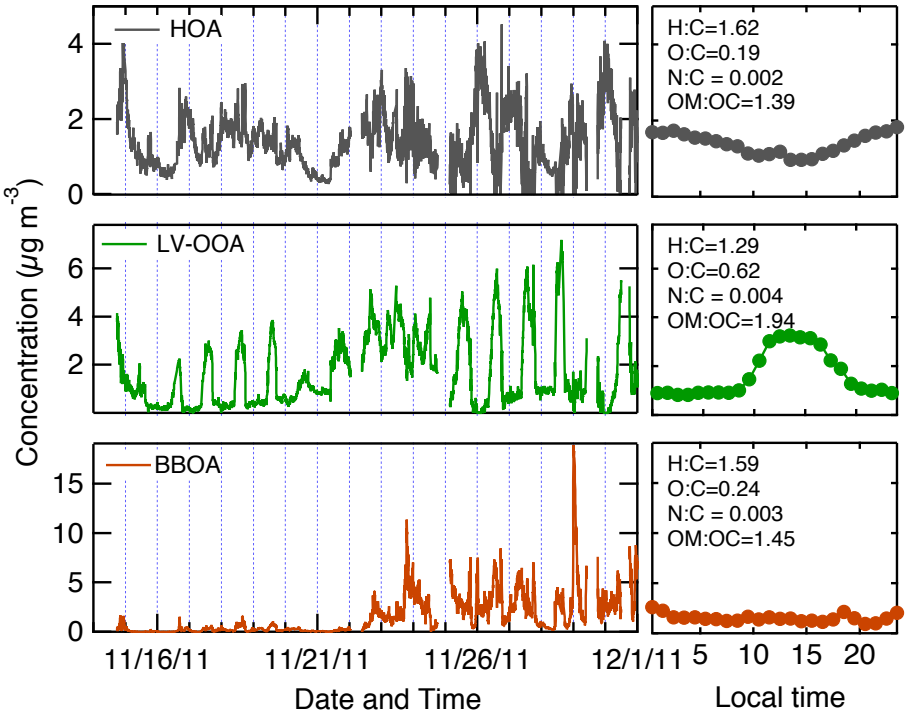

Fig. 3. Time series of HOA (grey), LV-OOA (green), and BBOA (brown) and their diurnal time trend.

ACPD
14, 4787–4826, 2014

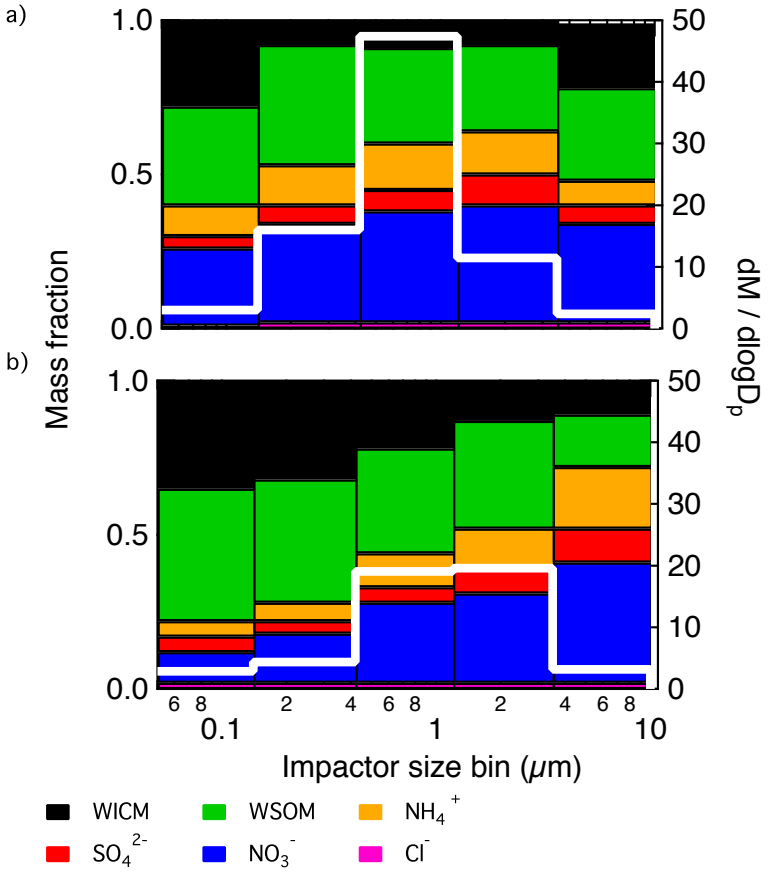

Fig. 4. Size resolved average aerosol composition and mass size distribution (white line) during day time (09:00–18:00, **a**) and during night time (18:00–09:00, **b**).

ACPD
14, 4787–4826, 2014

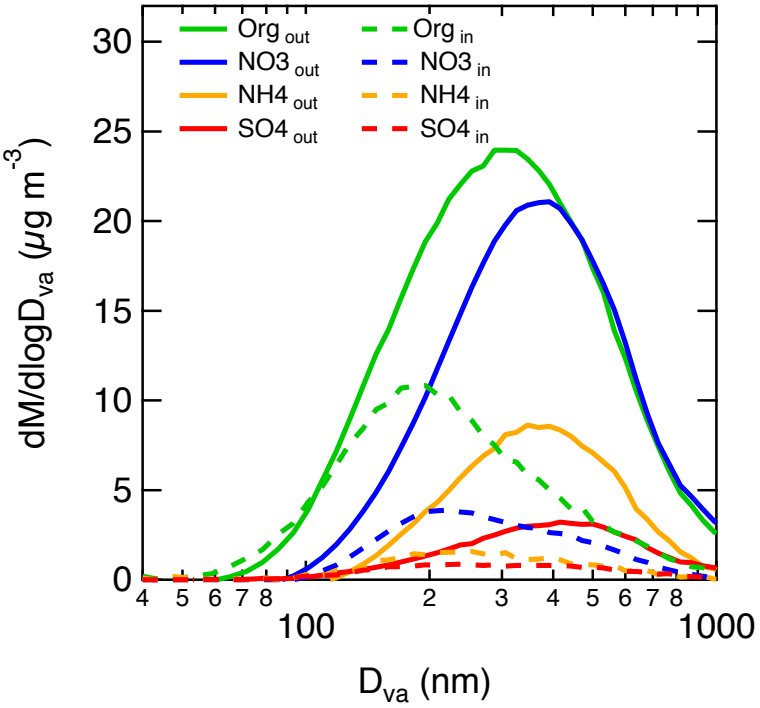

Fig. 5. Mass size distribution of major constituents of submicron particle out of fog (straight line) and in fog (dotted line) averaged over the entire campaign.

ACPD
14, 4787–4826, 2014

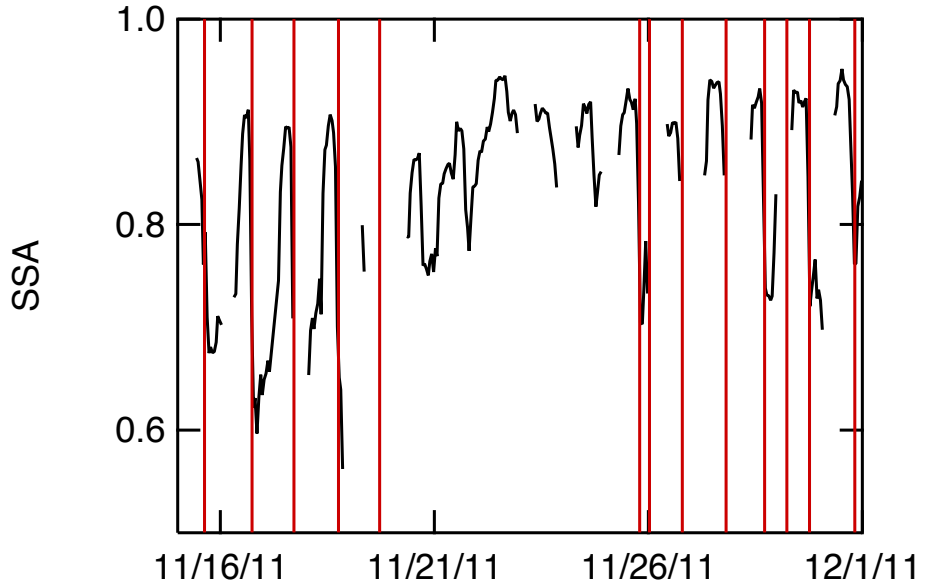

Fig. 6. Time trend of Single Scattering Albedo (SSA) at 573 nm; red vertical lines identify the beginning of fog events.

ACPD
14, 4787–4826, 2014

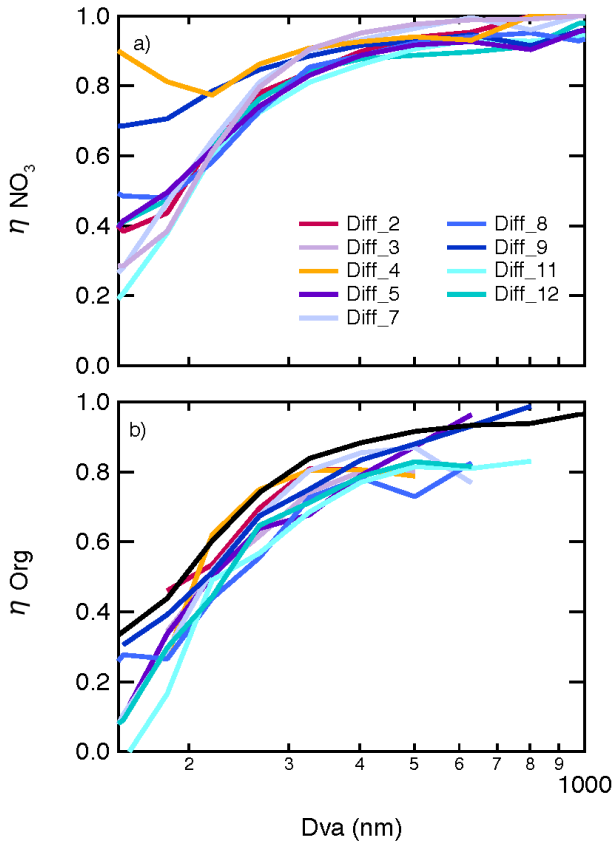

Fig. 7. Mass scavenging efficiency (η) size distribution of nitrate **(a)** and organics **(b)** for each fog event; black line in **(b)** corresponds to average nitrate scavenging efficiency. D_{va} is vacuum aerodynamic diameter.

ACPD
14, 4787–4826, 2014

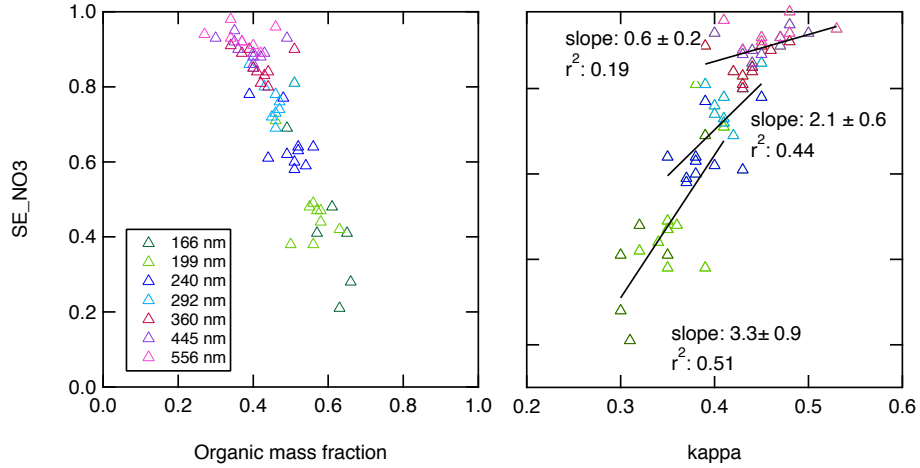

Fig. 8. Size segregated scavenging efficiency of nitrate as a function of organic mass fraction **(a)** and κ **(b)**; markers are color coded as a function of particle diameter (D_{va}).

ACPD
14, 4787–4826, 2014

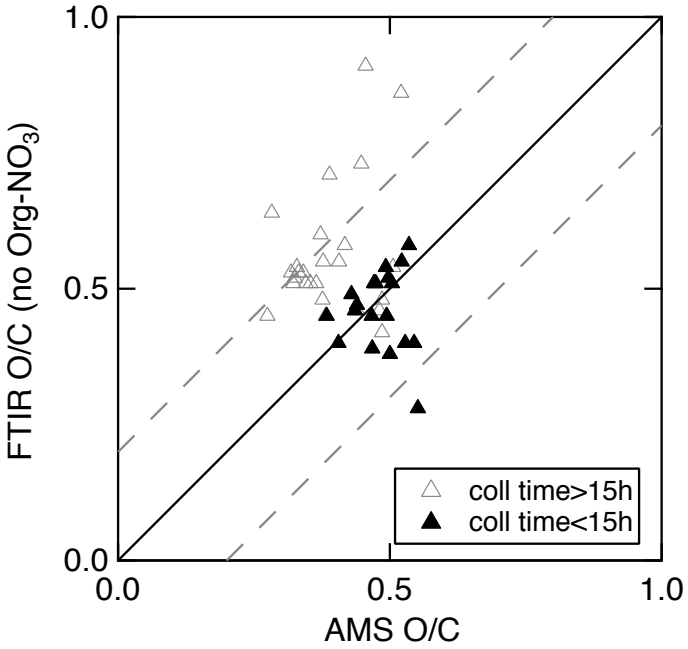

Fig. 9. Comparison of oxygen to carbon ratio from analysis of organic aerosol by FTIR and AMS. For the comparison, FTIR ratio is calculated ignoring the contribution of organonitrate. Black triangles are samples with collection time below 15 h.

ACPD
14, 4787–4826, 2014